remote sensing

MDPI

Article

Analysis of the Spatial and Temporal Patterns of Ground-Level Ozone Concentrations in the Guangdong–Hong Kong–Macao Greater Bay Area and the Contribution of Influencing Factors

Xi Tan [1], Yun Qian [1], Han Wang [1,2], Jiayi Fu [1] and Jiansheng Wu [1,2,*]

[1] Key Laboratory for Urban Habitat Environmental Science and Technology, School of Urban Planning and Design, Peking University, Shenzhen 518055, China
[2] Laboratory for Earth Surface Processes, Ministry of Education, College of Urban and Environmental Sciences, Peking University, Beijing 100871, China
* Correspondence: wujs@pkusz.edu.cn; Tel.: +86-755-26032282 or +86-755-26035508

Abstract: Ozone (O_3) pollution has negative impacts on human health and property. The Guangdong–Hong Kong–Macao Greater Bay Area (GBA) is facing severe O_3 pollution problems due to rapid economic development. In this paper, we used sensitivity experiments and GeoDetector to analyze the effects of meteorological factors, anthropogenic emissions, and landscape patterns on O_3 concentrations as well as the contributions of NO_x and NMVOC (non-methane volatile organic compounds) to the variation of O_3 concentrations and the causes of sectoral emissions in the GBA in 2017. The results revealed that, in GBA, the contribution of meteorology to the variation of O_3 concentration was dominant both in terms of region and extent, and the contribution of emissions was relatively weak. The contribution of meteorology and emissions to O_3 production was mainly contributory. Meteorology contributed significantly to O_3, and its non-linear interaction with anthropogenic emissions and surface landscape affected O_3 concentration changes. The degree of contribution of NO_x and NMVOC varied widely among seasons, and the variation of their relative contribution areas was related to residential sector emissions and agricultural sector emissions. This article enriches the exploration of the O_3 formation mechanism in the GBA and provides theoretical support for the implementation of differentiated regional and seasonal mitigation strategies for O_3 concentration.

Keywords: meteorology; anthropogenic emissions; landscape pattern; sensitivity experiments; ozone concentration

Citation: Tan, X.; Qian, Y.; Wang, H.; Fu, J.; Wu, J. Analysis of the Spatial and Temporal Patterns of Ground-Level Ozone Concentrations in the Guangdong–Hong Kong–Macao Greater Bay Area and the Contribution of Influencing Factors. *Remote Sens.* **2022**, *14*, 5796. https://doi.org/10.3390/rs14225796

Academic Editor: Manuel Antón

Received: 26 October 2022
Accepted: 15 November 2022
Published: 16 November 2022

1. Introduction

Tropospheric ozone (O_3) is a component of photochemical smog. Long-term or short-term exposure to O_3 will have an impact on pulmonary function and the cardiovascular and nervous systems [1,2], resulting in premature death, the reduction of crop productivity, and economic losses [3–6]. During 2015–2019, sulfur dioxide (SO_2), nitrogen dioxide (NO_2), PM (particulate matter), and carbon monoxide (CO) mean annual concentrations in Chinese urban environments showed a downward trend, while the mean annual concentration of O_3 increased by 4.7% [7–10]. Surface O_3 pollution has become a major air pollution problem in many cities in developing China [11]. Elucidating the O_3 spatial mechanism of generation and dispersion is important for developing effective strategies.

Meteorology is a major aspect driving O_3 production [12,13], where temperature, total precipitation, relative humidity, surface pressure, and wind speed are important variables affecting its concentration [14–18]. Surface O_3 is formed by complex photochemical reactions involving atmospheric nitrogen oxides (NO_x), volatile organic compounds (VOCs), and methane [19]. Due to the complex response of O_3 to meteorology and precursor emissions, the influence of these variables (and their interactions) on surface O_3 varies significantly with season and region [16,20]. In addition, land use, which reflects the intensity of human activities, also alters the production and cycling characteristics of O_3 [14]. However, most current studies on the role of land use on air pollution focus on the effects on particulate matter ($PM_{2.5}$, PM_{10}) concentrations [21–24], and there are fewer studies on the effects of land use landscape patterns on O_3.

Sensitivity experiments are often used in air pollutant analyses, which are simulated by chemical transport models (e.g., the GEOS Chem, WRF-CMAQ model) [12,25–28]. On the basis of emission inventory and meteorological data, the contribution of factors can be obtained by simulating pollutant concentration values in two or more periods. The neural network is a statistical model prediction method and an effective tool used to describe variation in nonlinear phenomena [29], which is characterized by simple calculations, low data requirements, and high accuracy [30]. Using this method to predict and simulate air pollutants, it is possible to obtain a nonlinear prediction and simulation within a short period, without needing a large amount of meteorological and anthropogenic emission data. Moreover, most of the studies conducted sensitivity experiments over many years or the same period of two years, and there is less seasonal analysis within one year.

Currently, the methods adopted to explore the impact of environmental conditions on the variation of O_3 concentration include multiple linear regression [31–33], quantile regression [31,33], principal component analysis [32], Kolmogorov–Zurbenko (KZ) filtering [34], and convergence cross-mapping [35]. The GeoDetector method has been widely used to study the interaction among air pollution factors, which could overcome collinearity and quantify the influence of single factors and their interactions [16]. O_3 formation involves photochemical reactions and nonlinear responses between most meteorological variables [36,37], primary pollutants such as NO_x and VOC [38], and aerosols and O_3 [39]. Coupled with the fact that high urban temperature can have direct or indirect effects on O_3 and VOC concentrations [40], it becomes increasingly important to investigate the effects of urban O_3 concentrations using nonlinear models.

As an important leading region for China's economic growth, the Guangdong–Hong Kong–Macao Greater Bay Area (GBA) has seen rapid urban development in recent years, followed by increasing ground-level O_3 pollution [41]. This paper investigates the seasonal dominant factors affecting the ground O_3 in the GBA and explores the effects of meteorological variables, anthropogenic emissions variables, and landscape patterns on the O_3 concentration. In this paper, we first designed four sets of sensitivity experiments based on the back propagation (BP) neural network to identify the dominant factors in different seasons and explored the sensitivity zoning of NO_x and NMVOC affecting O_3. Then, the GeoDetector model was used to quantify the contribution of anthropogenic emissions, meteorological variables, and landscape patterns (and their interactions) to surface O_3 concentrations. The contribution of sectoral emissions affecting NO_x and NMVOC sensitivity was also explored.

2. Materials and Methods

2.1. Study Area

The GBA is a metropolitan district located in southern coastal China (Figure 1), which consists of 11 cities including 4 international megacities, namely Guangzhou, Shenzhen, Hong Kong, and Macau. The GBA measures approximately 56,000 km^2 and has a permanent population of more than 70 million (http://www.cnbayarea.org.cn, accessed on 21 July 2022). According to the "Guangdong–Hong Kong–Macao Pearl River Delta Regional Air Monitoring Network 2019 Monitoring Results Report", air pollutants, e.g., SO_2, NO_2, PM_{10}, CO, and $PM_{2.5}$, showed a downward trend from 2015 to 2019, while the annual mean O_3 concentration increased by 28%. Prevention and control of O_3 pollution have become one of the major environmental challenges facing the GBA.

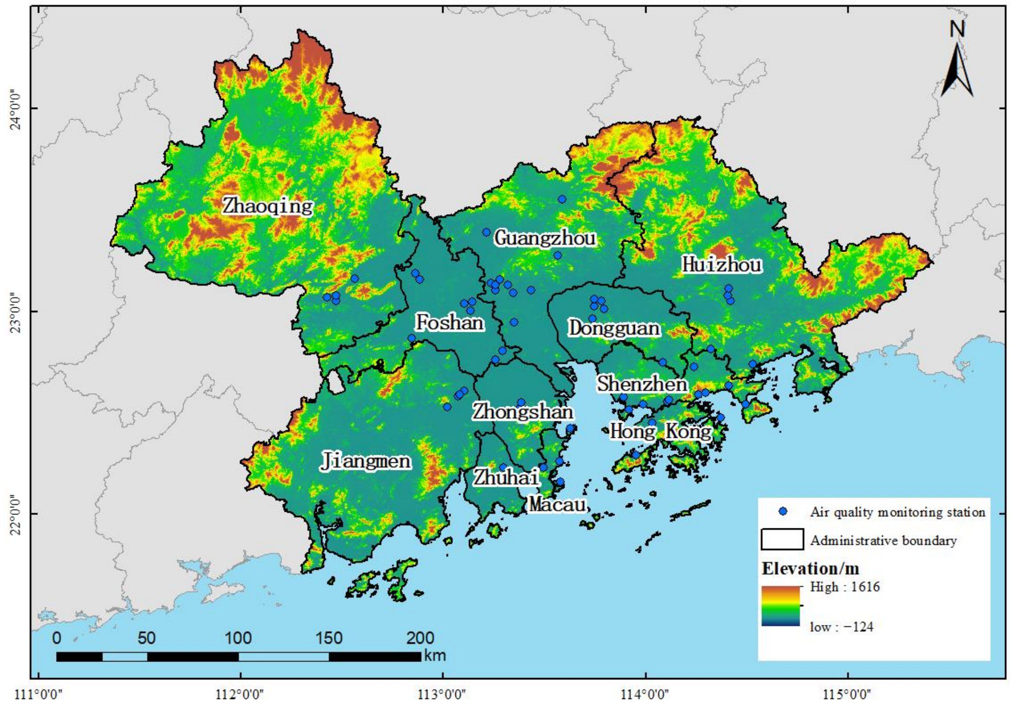

Figure 1. Spatial distribution of the monitoring sites in the study area.

2.2. Data

A fishing net with a resolution of 0.25° × 0.25° was generated in ArcGIS 10.4 (Developed by ESRI, Inc. from Redlands, CA, USA.) as a basic research unit for data aggregation. Then, the O_3 concentration level, the values of anthropogenic emission, and meteorological variables were separately counted in each fishing net for the 118 grids covering GBA. The land cover of each grid was intercepted and calculated in Fragstats 4 to obtain the corresponding landscape metrics.

2.2.1. Ground-Level O_3

The O_3 hourly concentration monitoring data for mainland China were obtained from the Urban Air Pollution Monitoring Network (https://quotsoft.net/air/, accessed on 10 November 2021) established by the China National Environmental Monitoring Center. Additionally, the monthly O_3 concentration data for stations in Hong Kong and Macau were derived from the regional air monitoring network of Guangdong, Hong Kong, and Macao in the Pearl River Delta. The daily average O_3 concentration was obtained by averaging the 24 h O_3 concentrations. Since there are different degrees of missing O_3 h in each month, the days with less than 12 h of missing concentration were excluded, and the daily average O_3 concentrations of the remaining effective days were averaged to obtain the monthly average O_3 concentration. The distribution of the 61 monitoring stations in the GBA is shown in Figure 1.

The Chinese high-resolution air pollution reanalysis dataset [42] was provided by the Institute of Atmospheric Physics. The dataset had a high temporal and spatial resolution, the latter reaching 15 km [43]. In this study, we used the monthly O_3 data derived from the atmospheric reanalysis dataset for the period between January and December 2017. The data were processed and displayed in ArcGIS with a spatial resolution of 0.17° (approximately 20 km), which met other data resolution sizes in this paper. To obtain O_3 data with spatial continuity and high accuracy, we used monitoring data to fuse the data. The details for the method can be found in Section 2.3.1.

2.2.2. Emission Inventory Data

The anthropogenic emission variables were obtained from the Chinese Multi-scale Emission Inventory Model (MEIC, http://meicmodel.org/, accessed on 10 November 2021) developed at Tsinghua University. The resolution of the inventory data is 0.25° × 0.25°. In this study, the 2017 emission inventory was selected, which included 10 emissions from 5 sectors, including NMVOC, SO_2, $PM_{2.5}$, PM_{10}, organic carbon (OC), NO_x, NH_3, CO_2, CO, black carbon (BC), etc., from transportation, residential, electricity, industry, and agriculture.

2.2.3. Atmospheric Reanalysis Dataset

In this study, the ERA-5 assimilation analysis dataset, of the European Center for Medium-Range Weather Forecast (ECMWF, https://www.ecmwf.int/en/forecasts/datasets, accessed on 10 November 2021), was selected, with a resolution of 0.25° × 0.25°.

The temperature at 2 m (T, °C), wind speed at 10 m (WS, m s^{-1}), relative humidity (RH, %), ground pressure (PS, hPa), and total precipitation (TP, mm) were selected as the meteorological variables. Since the dataset showed that the number of sunshine hours in the study area was the same, the index of sunshine hours was excluded. As ERA-5 does not include relative humidity data, this parameter was calculated using Equation (1), on the basis of the provided dew point and surface temperature values at 2 m above the surface [44]:

$$RH = \frac{e^{\frac{17.625 \times T_{dc}}{(243.04 + T_{dc})}}}{e^{\frac{17.625 \times T_c}{(243.04 + T_c)}}} \times 100\% \quad (1)$$

where T_{dc} is the dew point temperature (°C), T_c is the actual temperature (°C), and RH is the relative humidity (%).

2.2.4. Land Cover

The land cover data were obtained from the 2017 global land cover dataset (FROM-GLC30) collected by Tsinghua University, with a resolution of 30 m. After strict verification, the data accuracy was estimated at 72.35% [45]. The land cover types that characterize the GBA include cropland, forest, grassland, shrubland, wetland, water, impervious surface, and bare land. The detail is shown in Figure 2.

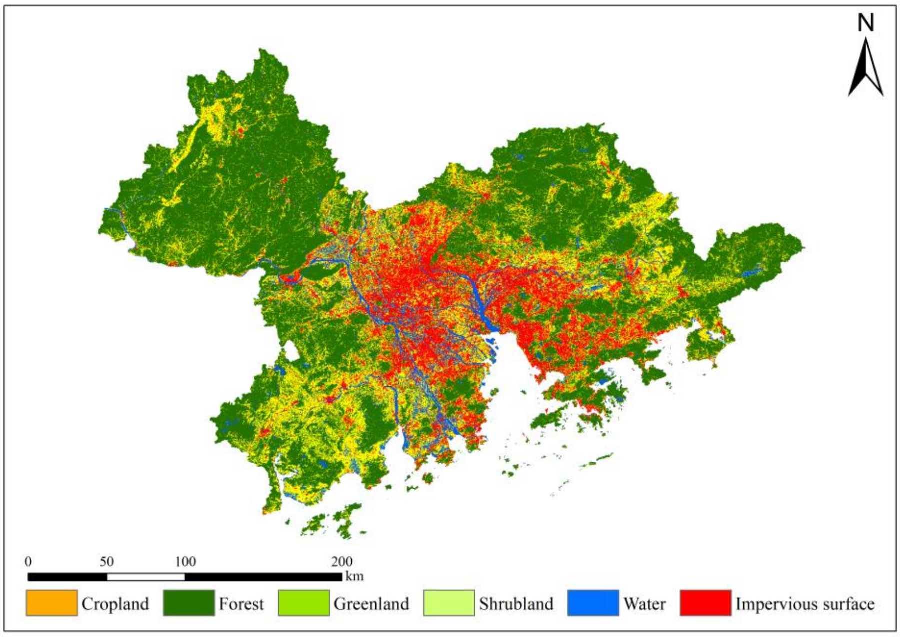

Figure 2. Land cover types in the GBA.

2.3. Methods

The flow chart of the study is shown in Figure 3. Firstly, the data was pre-processed. Secondly, sensitivity experiments on the basis of the BP network were performed to calculate the spatial distribution of the contribution of meteorological and emission factors to O_3, and then the GeoDetector model was used to refine the contribution of meteorology, emission, and landscape variables to regional O_3.

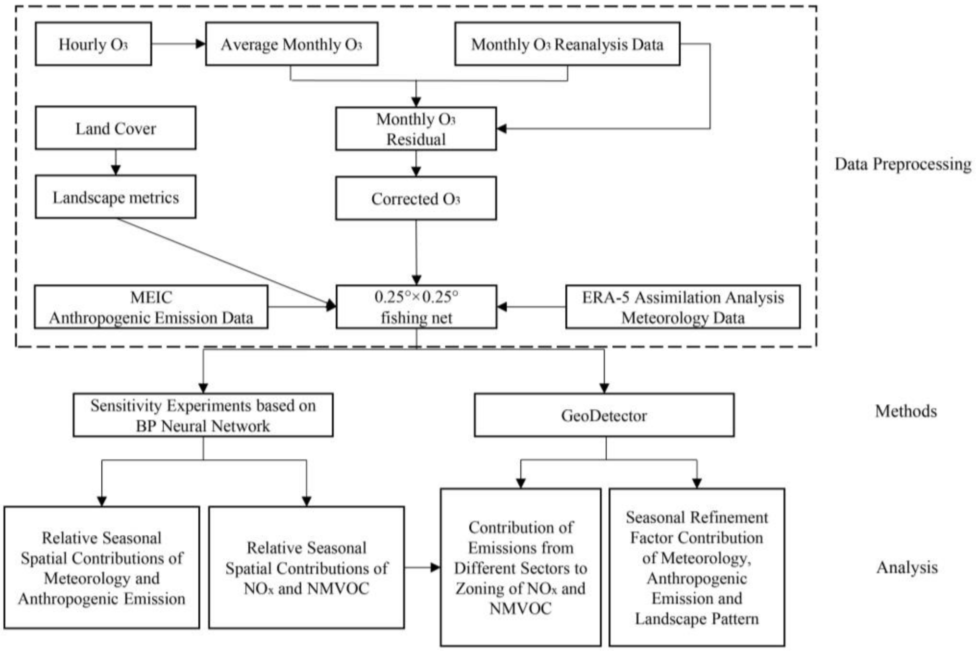

Figure 3. Research Flowchart.

2.3.1. Data Fusion

Since the monitoring stations of air pollution reanalysis data did not include some areas of Hong Kong and Macao [43], the data of monitoring stations were used to correct the air pollution data for the GBA. The specific steps are as follows [46]. First, the monthly monitoring station data values were subtracted from the O_3 reanalysis data values to calculate the monthly concentration residuals at the monitoring locations, then ordinary kriging interpolation was performed on the concentration residuals to generate a 0.17° × 0.17° monthly concentration residual map. Finally, the monthly residual interpolation values were added to the reanalysis data grid to obtain the corrected monthly concentrations for each grid. The calculation equation is as follows.

$$r_i = m_i - a_i \tag{2}$$

$$\hat{C}_j = a_j - \hat{r}_j \tag{3}$$

where r_i is the monthly concentration residual of monitoring point i, m_i is the monthly monitoring data of monitoring point i, a_i is the monthly O_3 reanalysis value on the grid corresponding to monitoring point i, a_j represents the monthly O_3 reanalysis value on grid j, $\hat{r}_j$ is the monthly residual after interpolation on grid j, and $\hat{C}_j$ represents the monthly corrected O_3 on grid j.

2.3.2. Landscape Metrics

Landscape metrics highly condense the information on landscape patterns, effectively reflecting the composition and spatial configuration of the landscape structure. In this study, several landscape metrics were selected to quantify the landscape pattern in the GBA. Table 1 describes in detail the selected landscape indicators, which were: landscape area (LPI), landscape shape (LSI, SHAPE_MN), landscape diversity (SHDI, CONTAG), and landscape agglomeration (AI).

Table 1. Ecological meanings of the selected landscape metrics.

Index Properties	Indicators	Ecological Meaning
Area and Margin	Largest Plaque Area (LPI)	Indicates the influence degree of the largest patch on the entire land cover type or landscape.
Shape	Landscape Shape Index (LSI)	Represents the total length of the boundary (multiplied by the square correction constant) divided by the square root of the total landscape area; the larger the value, the more complex the type.
	Mean Shape Index (SHAPE_MN)	The patch perimeter is divided by the smallest possible perimeter of the most compact patch, reflecting the complexity of the shape of a single patch.
Heterogeneity	Contagion Index (CONTAG)	Describes the non-randomness, or degree of agglomeration, of different patch types in the landscape.
	Shannon Diversity Index (SHDI)	Reflects the diversity of the landscape; the higher the value, the richer the diversity of the landscape.
Aggregation	Aggregation Index (AI)	Indicates the degree of aggregation of the landscape.

2.3.3. Sensitivity Analysis of Contribution

1. BP neural network model

A two-layer BP neural network was used for the simulations. The number ratio of the input layer, hidden layer, and output layer was 1:1:1. The tangent log sigmoid function was selected as the transfer function of the hidden layer, and the linear function was the transfer function of the output layer.

The input layer neurons were meteorological variables, emission variables, and landscape pattern variables. The number of neurons in the hidden layer was tested with 19 hidden layers and 5 neurons. The learning rate was set to 0.05 and the target error to 0.0001 for simulation. The BP network was trained using 119 rasters corresponding to January to December 2017 data from the study area (1428 in total). The model performance was evaluated using a tenfold cross-test, which divides all data into ten sub-samples, retaining one sub-sample each time as validation data, and the remaining nine sub-samples were used for model training. The process was repeated ten times to obtain R^2 and root mean square error (RSME) as indicators for evaluating model performance.

2. Experimental design and analysis

Four experiments (Table 2) were designed to simulate O_3 concentration at specific x (base time) and y (aim time) times [28]. The contributions of meteorology (NO_x) ($EXP_{y,x}$) and emission (NMVOC) ($EXP_{x,y}$) to O_3 concentration were quantified using the O_3 concentration simulated by different combinations of the same variables at x and y times. The simulated concentrations of x and y time were compared through a linear relationship to evaluate the contribution of meteorology (NO_x) and emission (NMVOC) to the change in O_3 concentration. The normalization contribution was then calculated. The formulas adopted are shown in Equations (4)–(7).

$$Con(Met/NO_x) = \frac{O_3EXP_{x,x} - O_3EXP_{y,x}}{O_3EXP_{x,x} - O_3EXP_{y,y}} \tag{4}$$

$$Con(Emi/NMVOC) = \frac{O_3EXP_{x,x} - O_3EXP_{x,y}}{O_3EXP_{x,x} - O_3EXP_{y,y}} \tag{5}$$

$$NCon(Met/NO_x) = \frac{Con(Met/NO_x)}{Con(Met/NO_x) + Con(Emi/NMVOC)} \tag{6}$$

$$NCon(Emi/NMVOC) = \frac{\mathrm{Con}(\mathrm{Emi}/NMVOC)}{\mathrm{Con}(\mathrm{Met}/NO_x) + \mathrm{Con}(\mathrm{Emi}/NMVOC)} \tag{7}$$

Table 2. BP network model used in the sensitivity contribution experiments.

Experiments	Description
$EXP_{x,x}$	Model run with meteorology (NO_x) at x time and emissions (NMVOC) at x time
$EXP_{y,x}$	Model run with meteorology (NO_x) at y time and emissions (NMVOC) at x time
$EXP_{x,y}$	Model run with meteorology (NO_x) at x time and emissions (NMVOC) at y time
$EXP_{y,y}$	Model run with meteorology (NO_x) at y time and emissions (NMVOC) at y time

$O_3EXP_{x,x,}$, $O_3EXP_{y,y}$, $O_3EXP_{y,x}$ and $O_3EXP_{x,y}$, respectively, represent the O_3 concentrations simulated by $EXP_{x,x}$, $EXP_{y,y}$, $EXP_{y,x}$, and $EXP_{x,y}$; $Con(Met/NO_x)$ and $Con(Emi/NMVOC)$ represent the contributions of meteorology and emission (NO_x and NMVOC), respectively; and $NCon(Met/NO_x)$ and $NCon(Emi/NMVOC)$ represent the normalized contributions of meteorology and emission (NO_x and NMVOC), respectively.

3. Analysis of sensitivity results and selection of base time

Four cases exist for the results obtained from $Con(Met)$ and $Con(Emi)$ calculated by Equations (4) and (5), respectively (Table 3).

Table 3. Sensitivity contribution results and corresponding meteorological conditions.

Result Value	Corresponding Range			Corresponding Results
I. $Con(Met) > 1$	$EXP_{y,y} > EXP_{y,x}$			Compared with the baseline, emission promotes a decrease in O_3 .
II. $Con(Met) < 1$	$EXP_{y,y} < EXP_{y,x}$	or	$EXP_{x,x} < EXP_{y,x}$	Compared with the baseline, emission promotes an increase in O_3 .
III. $Con(Emi) > 1$	$EXP_{y,y} > EXP_{x,y}$			Compared with the baseline, meteorology promotes a decrease in O_3 .
IV. $Con(Emi) < 1$	$EXP_{y,y} < EXP_{x,y}$	or	$EXP_{x,x} < EXP_{x,y}$	Compared with the baseline, meteorology promotes an increase in O_3 .

After statistical analyses, the grids with the lowest monthly O_3 concentration were selected as the base time y input models to make comparisons with other seasons.

2.3.4. Geode Ector

The GeoDetector software comprises a set of statistical methods that can detect spatial differentiation and reveal potential driving forces. Models can be performed to assess nonlinear relationships between potential factors and target geographic phenomena. The core idea at the base of the model assumption is that if an independent variable has an important influence on a dependent variable, then the spatial distribution of the two variables should be similar [47].

The spatial correlation of X (e.g., meteorological variables, anthropogenic emission variables, and landscape pattern variables) and Y (e.g., ground-level O_3 concentration) can be measured by q statistics, which are defined as:

$$q = 1 - \frac{\sum_{h=1}^{L} N_h \sigma_h}{N\sigma_h} = 1 - \frac{SSW}{SST} \quad (8)$$

$$SSW = \sum_{h=1}^{L} N_h \sigma_h \quad (9)$$

$$SST = N\sigma_h \quad (10)$$

where $h = 1, \ldots, L$ is the category of factor X, and N_h and N are the h category and sample size of the entire study area, respectively. SSW and SST are the sum of variance and total variance, respectively, of the h category and the entire study area. The value of q is [0, 1]. The greater the value of q, the higher the correlation with O_3. The effect of the interaction between two X variables on O_3 can also be quantified by q statistics.

3. Results

3.1. O_3 Concentration Temporal and Spatial Differentiation Characteristics

The corrected O_3 concentration value was verified by the monitoring data (Appendix A). The mean annual and seasonal O_3 distribution in the GBA for the year 2017 is shown in Figure 4. Based on the mean annual data, the areas with high O_3 concentrations were in the southeast of the GBA, specifically, southeast of Huizhou. The low-concentration areas were located in the northwest cities, such as Zhaoqing, Foshan, and part of Guangzhou, Jiangmen, and Hong Kong. Based on the mean seasonal data (a–d), O_3 concentration was the lowest in summer (mean 44.6 $\mu g/m^3$), followed by winter (mean 60 $\mu g/m^3$), spring (mean 60.2 $\mu g/m^3$), and was the highest in autumn (mean 62.8 $\mu g/m^3$). The spatial distribution of O_3 in the GBA was different between seasons: it was similar in spring, autumn, and winter when O_3 concentration was low in the northwest and high in the southeast, while it was different in summer, with low O_3 concentrations in the southeast, and high concentrations in the central areas.

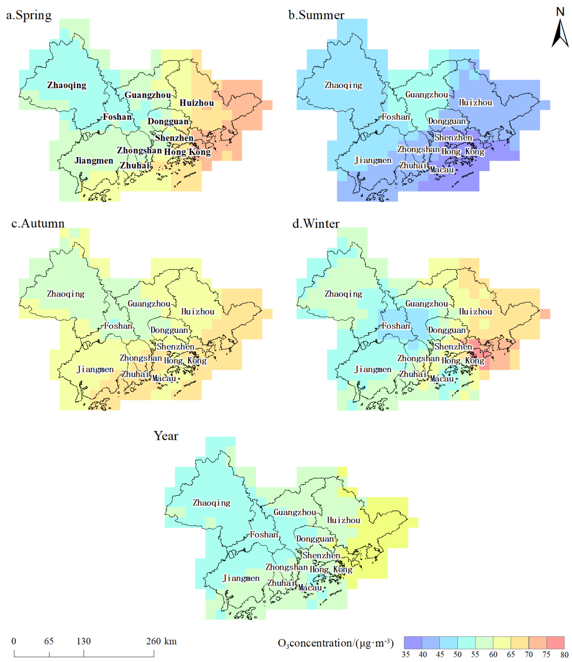

Figure 4. Average annual and seasonal distribution of O3 in the GBA in 2017. (**a**–**d**) represents the four seasons.

3.2. Sensitivity Experiments Results

3.2.1. Model Accuracy Verification

The BP network training results are shown in Table 4. The model reached the training goal after being trained 20 times, obtaining a total simulated decision coefficient (R^2) of 0.89. The coefficient of determination of seasons ranged from 0.4 to 0.8, and the simulation accuracy was poor in summer and winter. The decadal crossover results showed R^2_{CV} of 0.67 and RMSE of 7.53, and the model simulation accuracy was good.

Table 4. RSME of the BP network model.

	Year	Spring	Summer	Autumn	Winter	CV
R^2	0.89	0.81	0.51	0.78	0.40	0.63
RSME	8.31	6.64	4.86	5.27	7.06	0.79

3.2.2. Relative Contribution of Seasonal Meteorology and Emissions to O_3 Variation

Figure 5 shows the normalized contributions of meteorological factors and emissions for the four seasons obtained from the neural network simulation. The GBA was dominated by meteorological factors, the emission contribution was weak, and the distribution of normalized contribution size varied among the four seasons. The normalized contributions in spring, summer, and winter were similar, and the overall contribution of meteorological conditions to O_3 accounted for more than 60%. O_3 was most influenced by meteorological conditions in autumn. In summer, O_3 in the GBA was controlled mainly by meteorological conditions, and the meteorological factors normalized contribution decreased relative to other seasons, while the contribution of emissions was relatively higher. In spring, Jiangmen, Zhuhai, Zhongshan, Dongguan, Shenzhen, and Macao were relatively strongly controlled by meteorological factors, with the normalized contribution reaching more than 80%, while Zhaoqing, Foshan, Guangzhou, and Huizhou were relatively weakly controlled by meteorology, with the contribution of emissions ranging from 0 to 60%. In summer, Zhongshan and Foshan were subject to relatively high intensity of meteorological factors control, while Huizhou, Shenzhen, Hong Kong, Zhuhai, and Guangzhou were subject to relatively low intensity of meteorological factors control, with normalized contributions ranging from 0% to 60%. In the autumn, the overall contribution of meteorological factors to O_3 in the GBA reached more than 80%. In winter, except for central Huizhou, part of Guangzhou, Zhaoqing, Shenzhen, and other areas suffered from the role of emissions of 20% to 60%, and other areas suffered from the role of meteorological factors of more than 80%.

Figure 6 shows the contributions of meteorological factors and emissions obtained from sensitivity experimental simulations, and the direction of the meteorological, and emission contributions to O_3 can be inferred from the corresponding range of values (whether greater than 1) in Table 3. Regarding the meteorological factors, the meteorological factors in the GBA mainly show a facilitative effect on the production or accumulation of O_3 (*Con*(*Emi*) range was dominated by less than 1, corresponding to IV in Table 3). Regarding the emission factors, the four seasonal distributions of emission directions of action were relatively stable in the GBA. Compared with the baseline conditions, the emission conditions in Foshan, central Jiangmen, southern Zhaoqing, northern Guangzhou, and central Huizhou were unfavorable for the generation of O_3. Emission conditions in Zhongshan, southern Guangzhou, Zhuhai, central Zhaoqing, western Dongguan, and Jiangmen, except for the central part of the region, promoted the generation of O_3 (*Con*(*Met*) range is greater than 1 is dominant, corresponding to II in Table 3). The emission conditions in Shenzhen and Macau were not conducive to O_3 generation in spring, autumn, and winter, and showed a promotional effect in summer.

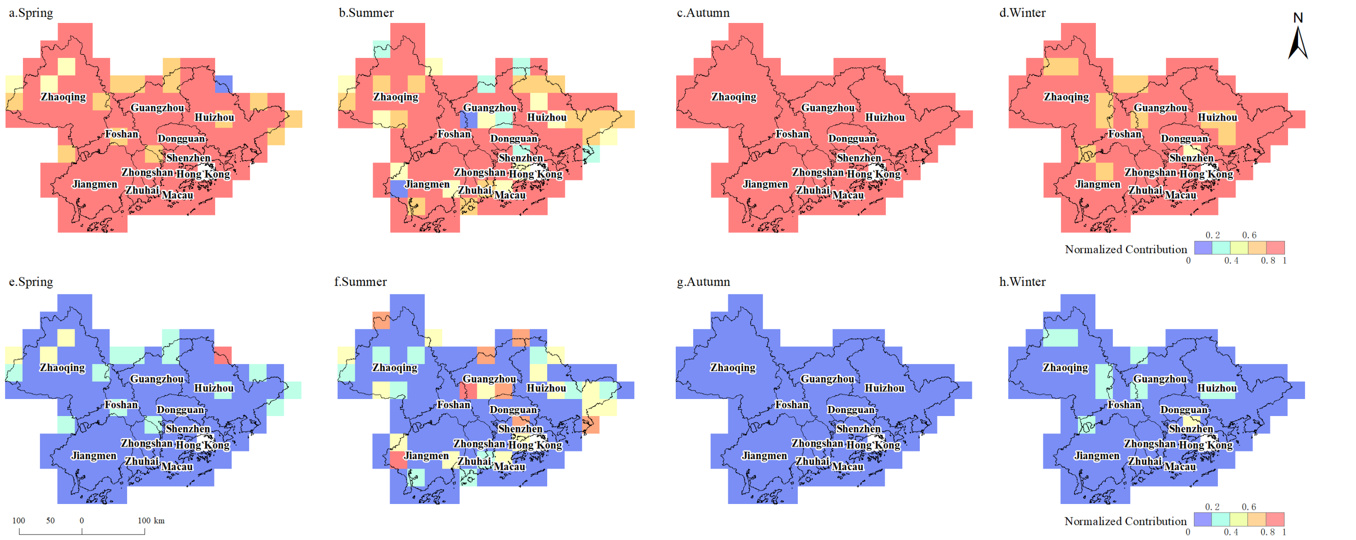

Figure 5. Distribution of the normalized contribution of seasonal meteorology and emission in the GBA. (**a**–**d**) for normalized meteorological contributions and (**e**–**h**) for normalized emission contributions).

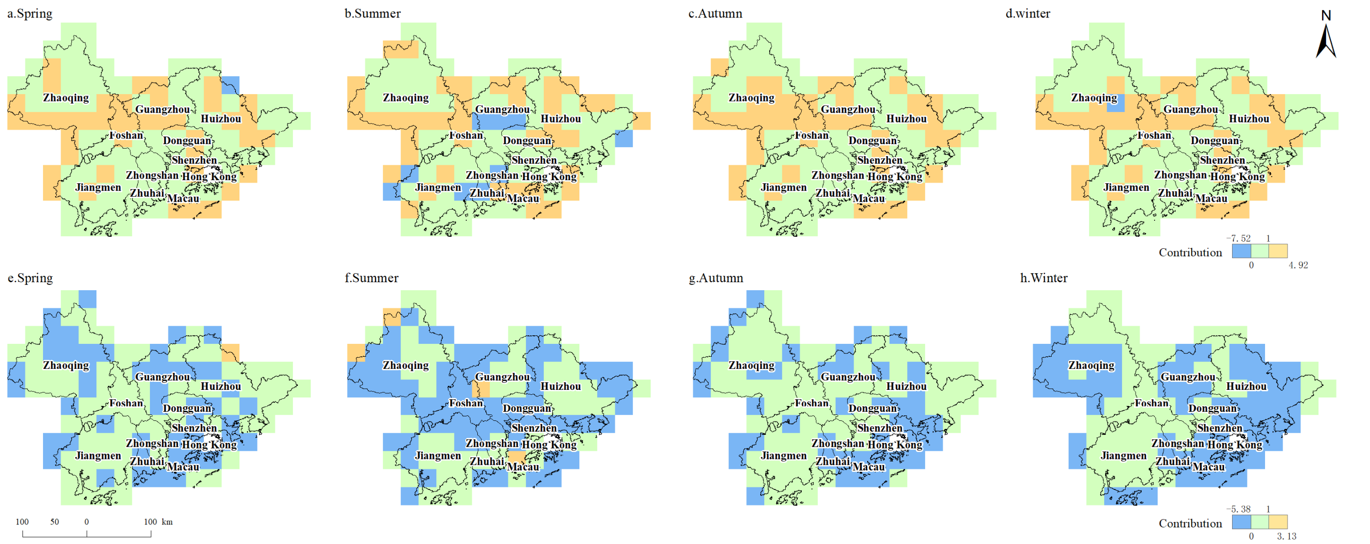

Figure 6. Distribution of the contribution degrees of seasonal meteorology and emission in the GBA. (**a**–**d**) for meteorological contribution and (**e**–**h**) for emission contribution).

3.2.3. Relative Contribution of Seasonal NO_x and NMVOC to O_3 Variation

The sensitivity simulation results of NO_x and NMVOC show (Figure 7) that the degree of contribution of NO_x and NMVOC varied greatly in different seasons. In terms of the relative contribution of NO_x and NMVOC, the overall O_3 concentration in the GBA in spring was influenced by NMVOC, with the NCon(NMVOC) reaching more than 60% in southern Zhaoqing, southern Foshan, Dongguan, northern Jiangmen, and south-central Huizhou, and more than 60% in coastal areas such as eastern Huizhou, Zhuhai, Macao, and Hong Kong. The impact of NO_x emissions on O_3 concentrations in the GBA was greater in summer, with Zhaoqing, Huizhou, Macau, Hong Kong, western Jiangmen, northern Guangzhou, southern Zhongshan, western Foshan, Shenzhen, and eastern Dongguan having more than 60% of NCon(NO_x), while Zhuhai was influenced mainly by NMVOC. In autumn, O_3 generation in the Greater Bay Area was influenced by NMVOC, and NCon (NMVOC) reached more than 60% in most areas of Zhaoqing, Foshan, Huizhou, Zhongshan, central Jiangmen, and eastern Dongguan. O_3 in the northern end of Zhaoqing, eastern

Foshan, and eastern Jiangmen were influenced mainly by NO_x emissions, and the relative contribution of NO_x and NMVOC in the rest of the region was not significant. In winter, the southeastern part of the GBA O_3 was affected mainly by NO_x emissions, with Zhuhai, Dongguan, Shenzhen, Hong Kong, Macau, Guangzhou, southern and northern Huizhou, and central Foshan being more obvious, while the northwestern was affected mainly by NMVOC, with Zhaoqing as the representative.

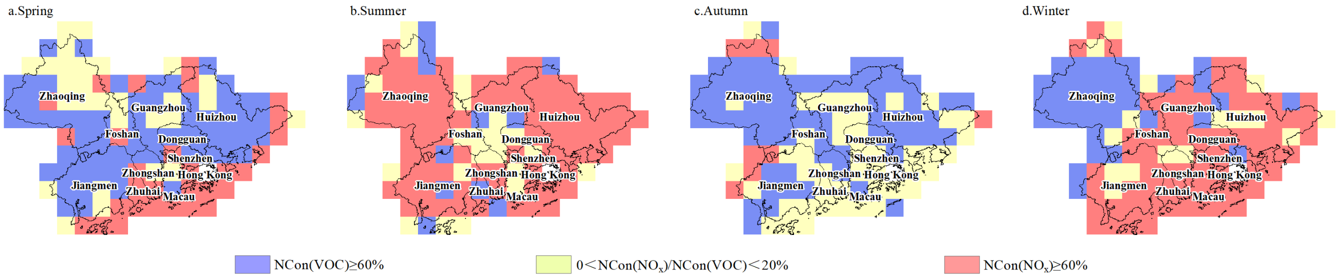

Figure 7. Distribution of the normalized contribution of seasonal NO_x and NMVOC in the GBA. (**a–d**) represents the four seasons.

3.3. GeoDetector Results

3.3.1. Analysis of the Factors Driving O_3 Concentration

Factor detectors were used to detect the contribution of 2017 and four-season drivers to O_3 concentrations (Table 5). The significant effects on O_3 were due almost solely to the meteorological factors, and the significant effect of meteorological factors on O_3 varied from season to season. Throughout the year, the most significant contributions to O_3 were T and TP, with q values of 0.35 and 0.31, respectively, followed by RH and WS, with q values of 0.18 and 0.12, respectively, and SP, with the least contribution of 0.06. In spring, the meteorological effects on O_3 were reflected mainly in T (q = 0.62), WS (q = 0.35), and TP (q = 0.17), and their *p*-values were also less than 0.01. The related directions of action showed that high temperature, low wind speed, and more precipitation in spring were the main reasons for promoting O_3 formation. In summer, the meteorological effect on O_3 was reflected mainly in TP (q = 0.41) and RH (q = 0.21), which also showed an opposite effect with O_3 concentration, indicating that more precipitation and higher humidity in summer were the reasons for inhibiting O_3 formation. In addition, LSI also showed a significant effect at the 0.05 level (q = 0.11), showing that the more complex the landscape type, the more it suppressed the concentration of summer O_3. In autumn, the meteorological factors, which were mainly in T (q = 0.68), had a more significant effect on O_3 concentration, and showed a homogeneous effect with O_3 concentration, indicating that the higher temperature in autumn in the GBA was responsible for the formation of O_3. In winter, O_3 concentration was controlled mainly by RH (q = 0.14) and SP (q = 0.17), suggesting that higher humidity and lower air pressure in winter were not conducive to ozone production. In addition, the landscape pattern factor CONTAG (q = 0.09) was also related to O_3 concentration, showing that the aggregation of different types of patches was not conducive to higher O_3 concentration in winter.

Table 5. The q statistics and correlation direction of the factors driving O3 concentration in the GBA. Positive and negative signs in parentheses represent the direction of the correlation.

Factors	2017	Spring	Summer	Autumn	Winter
WS	(+)0.12 **	(−)0.35 **	(−)0.11	(+)0.12	(+)0.11
SP	(+)0.06 **	(+)0.04	(−)0.17	(−)0.01	(+)0.17 *
T	(−)0.35 **	(+)0.62 **	(+)0.04	(+)0.68 **	(+)0.15
RH	(−)0.180 **	(−)0.08	(−)0.21 *	(−)0.20 **	(−)0.14 **
TP	(+)0.31 **	(+)0.17 **	(−)0.41 **	(+)0.09	(+)0.10
BC	(+)0.01	(+)0.05	(−)0.04	(+)0.01	(+)0.08
CO	(−)0.01	(+)0.06	(−)0.05	(+)0.01	(+)0.11

Table 5. *Cont.*

Factors	2017	Spring	Summer	Autumn	Winter
CO_2	(+)0.01	(+)0.06	(−)0.05	(+)0.01	(+)0.11
NH_3	(−)0.02	(+)0.08	(−)0.04	(−)0.01	(+)0.06
NO_x	(+)0.01	(+)0.07	(−)0.05	(+)0.01	(+)0.10
OC	(+)0.01	(+)0.04	(−)0.03	(+)0.01	(+)0.05
$PM_{2.5}$	(+)0.01	(+)0.06	(−)0.04	(+)0.01	(+)0.07
PMcoarse	(+)0.01	(+)0.05	(−)0.04	(+)0.01	(+)0.07
SO_2	(+)0.01	(+)0.05	(−)0.04	(+)0.01	(+)0.08
NMVOC	(+)0.01	(+)0.06	(−)0.04	(+)0.02	(+)0.08
LPI	(−)0.01	(−)0.02	(+)0.07	(−)0.01	(−)0.08
LSI	(+)0.01	(+)0.05	(−)0.11 *	(+)0.01	(+)0.14
SHAPE_MN	(+)0.01	(+)0.03	(−)0.09	(+)0.01	(+)0.10
CONTAG	(−)0.01	(−)0.03	(+)0.08	(−)0.01	(−)0.09 *
SHDI	(+)0.01	(+)0.03	(−)0.09	(+)0.01	(+)0.09
AI	(−)0.01	(−)0.03	(+)0.08	(−)0.01	(−)0.11

**. Significantly correlated at the 0.01 level (bilaterally). *. Significantly correlated at the 0.05 level (bilaterally).

3.3.2. Interaction of Factors Affecting O_3 Concentration

The ecological detector shows whether the two factors interacted with each other on the variation of O_3 concentration. The results showed that the meteorological factors WS, T, RH, and TP interacted with anthropogenic emissions and landscape patterns to influence the O_3 concentration (Table A1). The interaction detector shows the strength of the interaction between the two factors on the O_3 concentration (Figure 8). It was evident that most of the factors showed a non-linear enhancement of O_3 concentration between the two, i.e., the interaction between the two factors had a greater effect on the O_3 concentration than the sum of the effects of the two factors alone. The interactions between meteorological factors and emission factors and landscape pattern factors were strong, with the strongest influence of the interaction between T and other factors, followed by TP and RH, and the least influence of the interaction between WS and SP and other factors.

Landscape patterns can alter local microclimate conditions. Combining Table 5 and Figure 8, it can be seen that the correlation direction of landscape pattern factors with O_3 and with T were the same, and the correlation direction of T with O_3 were also the same, while the correlation direction of landscape pattern factors O_3 and with RH were opposite, and the correlation direction of RH with O_3 was also opposite. It could be shown that the smaller the area of individual patches within the landscape pattern, the more complex the individual patch types, the lower the degree of aggregation of different patch types, and the higher the complexity and lower the aggregation of the overall landscape pattern formed, and there would be a non-linear interaction with the meteorological conditions of high temperature, high pressure, and low humidity, thus promoting the generation of O_3. LSI and SHAPE MN in landscape patterns interacted in different directions with TP and WS and with O_3.

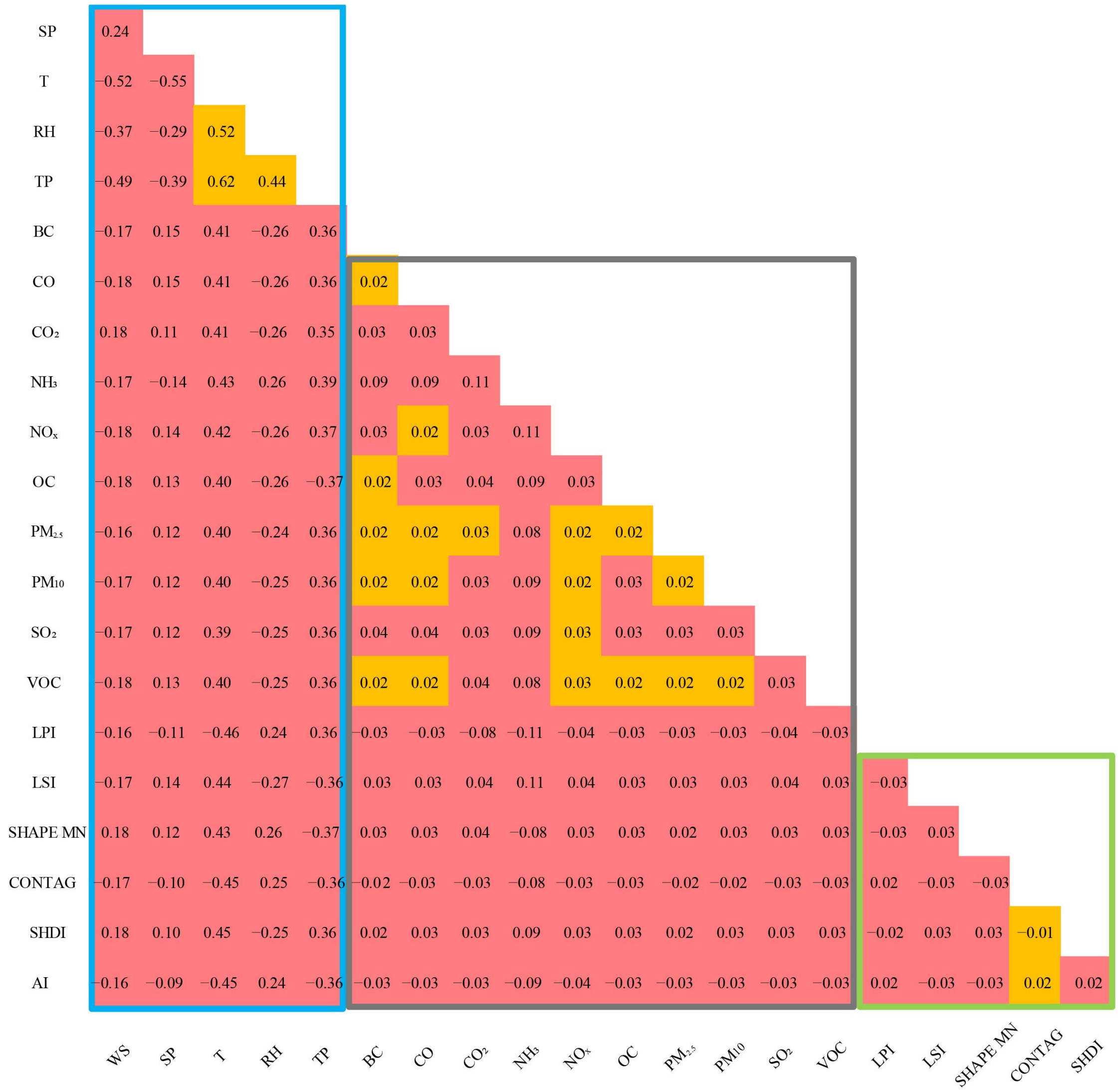

Figure 8. Strength of the interaction between meteorology, anthropogenic emission, and landscape patterns on O_3 concentrations. (Red represents non-linear enhancement, and orange represents double enhancement. The negative sign represents the opposite relationship between the two factors. Blue, grey, and green represent the interaction between each factor and meteorological, emission, and landscape pattern factors, respectively).

3.3.3. Detection of Emission Factors Affecting Seasonal NO_x and NMVOC Contributions

Factor detection of pollutant emission sector factors affecting the formation of NO_x and NMVOC contributing areas in different seasons was carried out (Table 6). The change in contribution was most sensitive mainly to the residential sector, followed by NH_3 emissions from the agricultural sector. The normalized contributions of NO_x and NMVOC in spring were influenced mainly by BC (q = 0.38), CO (q = 0.34), CO_2 (q = 0.27), NH_3 (q = 0.39), NO_x (q = 0.34), OC (q = 0.34), $PM_{2.5}$ (q = 0.34), PM_{10} (q = 0.33), and NMVOC (q = 0.3) emissions from the residential sector and also by CO_2 (q = 0.23) in the residential sector and NH_3 (q = 0.3) emissions in the agricultural sector. Only the q value of OC passed the significance test for the sectoral anthropogenic emission contribution partition in summer. In autumn, it was affected mainly by NO_x (q = 0.2), OC (q = 0.34), $PM_{2.5}$ (q = 0.34), PM_{10} (q = 0.33), and NMVOC (q = 0.3) in the residential sector. The NO_x and NMVOC contribution zoning affecting winter was similar to that of spring, but winter was not significantly affected by CO_2 and NH_3 emissions from the residential sector.

Table 6. Seasonal detection results of different sectoral emissions for NCon(NO_x) and NCon(NMVOC).

		BC				**CO**		
	Spring	**Summer**	**Autumn**	**Winter**	**Spring**	**Summer**	**Autumn**	**Winter**
Transportation	0.20 *	0.12	0.04	0.06	0.09	0.06	0.03	0.07
Residential	0.38 **	0.11	0.17	0.38 **	0.34 **	0.07	0.14	0.39 **
Power	0.14	0.07	0.06	0.10	0.14	0.12	0.08	0.10
Industry	0.12	0.06	0.07	0.05	0.14	0.09	0.09	0.04
Agriculture	/	/	/	/	/	/	/	/
		CO_2				**NH_3**		
	Spring	**Summer**	**Autumn**	**Winter**	**Spring**	**Summer**	**Autumn**	**Winter**
Transportation	0.09	0.06	0.03	0.07	0.09	0.06	0.03	0.07
Residential	0.27 **	0.10	0.15	0.07	0.39 **	0.09	0.15	0.28
Power	0.15	0.10	0.08	0.06	/	/	/	/
Industry	0.13	0.11	0.10	0.06	/	/	/	/
Agriculture	/	/	/	/	0.25 **	0.10	0.14	0.27 **
		NO_x				**OC**		
	Spring	**Summer**	**Autumn**	**Winter**	**Spring**	**Summer**	**Autumn**	**Winter**
Transportation	0.14	0.06	0.04	0.06	0.14	0.12	0.04	0.06
Residential	0.34 **	0.08	0.20 *	0.34 **	0.34 **	0.34 **	0.34 **	0.34 **
Power	0.11	0.11	0.07	0.11	0.11	0.11	0.11	0.11
Industry	0.14	0.12	0.08	0.06	0.13	0.13	0.13	0.13
Agriculture	/	/	/	/	/	/	/	/
		$PM_{2.5}$				**PM_{10}**		
	Spring	**Summer**	**Autumn**	**Winter**	**Spring**	**Summer**	**Autumn**	**Winter**
Transportation	0.14	0.19	0.14	0.14	0.14	0.14	0.14	0.14
Residential	0.34 **	0.07	0.34 **	0.34 **	0.33 **	0.33 **	0.33 **	0.33 **
Power	0.11	0.09	0.11	0.11	0.12	0.12	0.12	0.12
Industry	0.14	0.13	0.14	0.14	0.14	0.14	0.14	0.14
Agriculture	/	/	/	/	/	/	/	/
		SO_2				**NMVOC**		
	Spring	**Summer**	**Autumn**	**Winter**	**Spring**	**Summer**	**Autumn**	**Winter**
Transportation	0.08	0.08	0.08	0.08	0.09	0.09	0.09	0.09
Residential	0.09	0.09	0.09	0.09	0.30 **	0.30 **	0.30 **	0.30 **
Power	0.12	0.12	0.12	0.12	0.10	0.10	0.10	0.10
Industry	0.10	0.10	0.10	0.10	0.15	0.15	0.15	0.15
Agriculture					/	/	/	/

**. Significantly correlated at the 0.01 level (bilaterally). *. Significantly correlated at the 0.05 level (bilaterally).

4. Discussion

This paper first designed four sets of sensitivity experiments based on neural networks to explore the relative contributions of meteorological factors and anthropogenic emissions in four seasons. The results show that O_3 concentrations in the GBA were controlled mainly by meteorological factors, and the normalized contribution of meteorological factors reached more than 60% in all four seasons. Due to the GBA's location in the southern coastal region of China, changes in monsoon clouds might also lead to strong seasonality in ozone concentrations [48], and the meteorological influence on O_3 variability in the Bay Area was greater than in other regions [13]. Although the contribution of anthropogenic emission to the change in O_3 concentrations in the GBA during all seasons was relatively small, it was the main driver of the long-term upward trend in O_3 concentrations [49]. This paper also refined the spatial distribution of the direction of the contribution of meteorological and anthropogenic emission factors to O_3 production. The results show that meteorology in the four seasons had a major role in promoting O_3 concentrations in the GBA, and the distribution of emission factor on the production or accumulation of O_3 concentrations was more stable in the four seasons in the region of promotion and mitigation, and different emission measures should be considered for the two regions.

This article quantified the effects of small factors of meteorology, anthropogenic emission, and landscape pattern on O_3 concentrations, and the results showed that only meteorological factors had a significant effect on O_3 at the 0.01 level. Spring O_3 concentrations were related to wind speed, air temperature, and precipitation. Low wind and high-pressure stable atmospheric conditions limited convective mixing and ozone diffusion, and the weather pattern of increasing spring temperature was more conducive to accelerated O_3 production [50]. In addition, precursors from biomass emissions in the Indo–Burma region of the Southeast Asian subcontinent [51,52] and southwesterly winds at 850 hPa in spring [53] contributed to O_3 production, while the encounter with cold fronts or cold eddies may produce a certain amount of precipitation. The lowest O_3 concentration in the GBA in summer was related mainly to precipitation and humidity, and the presence of frequent typhoon storms and plum rains in summer brought clean ocean air, diluting high O_3 concentrations [16,54]. O_3 concentrations were highest in the GBA in autumn, and the results of this paper showed a significant relationship between temperature and humidity. The PRD was vulnerable to tropical cyclones and subtropical high pressure in autumn, and the ground conditions of enhanced solar radiation, higher temperatures, reduced cloudiness, and lower relative humidity were conducive to the photochemical reaction of O_3 [55]. Meanwhile, the stable atmospheric structure of the PRD at the periphery of typhoons was also conducive to the accumulation of O_3 [56]. In winter, the results showed a significant correlation between humidity and barometric pressure. In winter, northern winds prevailed in the GBA, dominated by the East Asian monsoon and influenced by the cold high pressure from the north, the humidity was lower in the GBA, and the temperature and radiation were also lower, which was not conducive to the photochemical reaction of O_3 [57], while the northern wind also brought in $PM_{2.5}$ pollutants, and the dimming effect of aerosols further inhibited the production of O_3 [58]. In addition, low O_3 air masses from the equatorial tropical low convergence zone transported by the East Asian local Hadley circulation can also reduce O_3 concentrations in areas such as Hong Kong [51].

Although the direct effect of urban landscape patterns on O_3 concentration was not very obvious, the results of the interaction detector showed that landscape pattern can interact with meteorological factors in a nonlinearly enhanced way to influence O_3 concentration changes. The smaller the area of individual patches, the more complex individual shape, the more complex the overall landscape shape, and the lower the degree of aggregation that would interact with the ground meteorological conditions favoring O_3 generation, such as high temperature, high pressure, and low humidity to promote O_3 generation., Thus, increasing the area utilized by individual site types, reducing the complexity of individual site shapes, and increasing the aggregation of different site types can suppress the generation of O_3. Additionally, these landscape pattern changes that favor O_3 formation also correspond to the development of urbanization [59]. It had been shown that the evolution of the urban heat island effect and changes in the thermal cycle caused by changes in urban structure due to urbanization and heat generated by anthropogenic heat sources can affect O_3 concentration [54,60–63]. Mitigating O_3 concentrations can also be achieved by introducing new landscapes to improve local microclimates. Studies have shown that the Wind-Corridor project can indirectly change meteorological factors, such as humidity, insolation, and evaporation by introducing more strong winds, thus reducing air pollution, while the project can also effectively mitigate the urban heat island effect [20,64], thereby reducing photochemical reactions. Therefore, the reduction of O_3 concentration can be achieved not only by reducing industrial activities and traffic inducement but also by changing the urban landscape pattern indirectly and permanently. The results of this paper also showed that landscape pattern factors, especially the interaction of individual patch shape and overall landscape type with wind speed and precipitation, were more complex for O_3 concentration.

This paper also quantified the relative contributions of NO_x and NMVOC to O_3 in the GBA. Compared with the NO_x/VOC limit—which indicates that as NO_x (VOC) concentration increases, O_3 concentration increases, and as VOC (NO_x) concentration increases [65], O3 concentration decreases—the relative contribution zone of NO_x (VOC) represents the greater effect of the increase or decrease of unit NO_x (VOC) concentration on the change of O_3 concentration in the region. The spatial distribution of the contributions in the four seasons varied substantially, with the GBA dominated by NMVOC contributions in spring and autumn, NO_x contributions in summer, and winter showing VOC contributions in the northwest and NO_x contributions in the southeast. The results of the study are similar to the results of Hu et al., with a moderate VOC-limited state in spring and autumn and a weaker VOC-limited state in summer. While Hu et al. showed a stronger VOC-controlled state in winter [66], the results of this paper showed a greater range of NOx contribution, a possible discrepant result that may be the result of different study scales and models or may be related to different quantitative focus (degree of impact and spatial extent of impact), but our results all suggest that seasonally different NO_x and VOC emission controls should be developed in GBA.

The results of this paper showed that emissions of CO, BC, NOx, OC, $PM_{2.5}$, PM_{10}, and NMVOC from the residential sector and NH_3 from the agricultural sector were the main factors influencing the changes in the relative contribution areas of NO_x and NMVOC. CO is one of the precursors of O_3, which can generate O_3 with hydrocarbons through HO_x and NO_x by radical catalytic reaction [55]. BC and CO may have a close source, and there was a good positive correlation between the two [67]. In addition, BC, OC, NH_3, $PM_{2.5,}$ and PM_{10} as aerosols and their precursors can also influence the photochemical reaction of O_3 by affecting UV radiation [68,69]. For emission sources, biomass combustion was the major source of NH_3, NO_x, CO, OC, and BC [70]. Biomass combustion, biogenic sources, paints/varnishes, and household solvents were also important sources of ambient VOC in the PRD region [71,72], and there was an enhancing trend of HCHO in some densely populated areas [73]. The results of this paper also emphasized the need for research on the mechanisms of O_3 formation from residential sector emissions in highly urbanized and densely populated areas, such as the GBA and the Yangtze River Delta region.

Considering that the dilution effect of wind speed on O_3 concentrations may have an impact in quantifying the contribution of local landscape pattern factors to O_3 concentrations, we additionally conducted experiments at different levels of wind speed, but the results showed little difference, so they are not discussed here (Table A2). The limitation of this work is that, firstly, in order to remedy the problem that the assimilation data of reanalysis data lack site data in Hong Kong and Macao, this paper used monitoring data to fuse with reanalysis pollution data, and this fusion method could be influenced by the distribution of sites, and the accuracy of O_3 concentration in areas with few sites may be impacted. Second, the landscape pattern of individual site types was not studied in this work. In addition, when studying the relationship between landscape patterns and environmental processes, multiple spatial scales should be selected to study or find the best study scale, but due to the limitation of data acquisition, only the highest accuracy of emissions was obtained as the scale for this paper, and further studies on this aspect will be considered in the future.

5. Conclusions

This paper studied the GBA and adopted sensitivity experiments and GeoDetector to analyze the dominant factors affecting O_3 and the contribution between each factor in 2017. The main findings are as follows.

The contribution of meteorology to O_3 concentration changes was dominant both in terms of region and extent, while the contribution of emissions was relatively weak, and both were dominant in contributing to O_3 production. Meteorology had a significant effect on O_3 concentrations. Although the direct effect of surface landscape on O3 was not obvious, it would have a nonlinear interaction with meteorological conditions to influence O_3 concentration changes, and the interaction between surface landscape patterns toward urbanization and favorable meteorological conditions promoted O_3 concentration generation or accumulation. Furthermore, the degree of contribution of NO_x and NMVOC in the GBA varied considerably in different seasons. Residential sector emissions and agricultural sector NH_3 emission were the main factors influencing the change in the relative contribution area of NO_x and NMVOC, related to a large amounts of precursors from biomass burning, biogenic sources, paint/varnish, and household solvents due to the dense population in the GBA. We provide support for the development of regionally and seasonally differentiated control strategies for the mitigation of O_3 concentration generation and production, as well as theoretical support for the mechanisms of urbanized surface landscape effects on O_3 concentration. The impact of emissions from the residential sector on O_3 sensitivity is also highlighted.

Author Contributions: Conceptualization, data curation, software, visualization, validation, writing—original draft, X.T.; methodology, validation, supervision, Y.Q.; validation, writing—review and editing, supervision, H.W.; software, validation, supervision, J.F.; conceptualization, resources, funding acquisition, J.W. All authors have read and agreed to the published version of the manuscript.

Funding: This study was funded by Shenzhen Fundamental Research Program, grant number GXWD20201231165807007-20200816003026001.

Data Availability Statement: The data in this study are open and can be made available to interested users upon contacting the corresponding author.

Conflicts of Interest: The authors declare no conflict of interest.

Appendix A

The corrected O_3 was more accurate. The coefficient of determination R^2 increased from 0.5 to 0.7 (Figure A1), root mean square error (RSME) decreased from 12 to 9.7, and normalized mean square error (NME) also decreased from 13.9% to 11.1%.

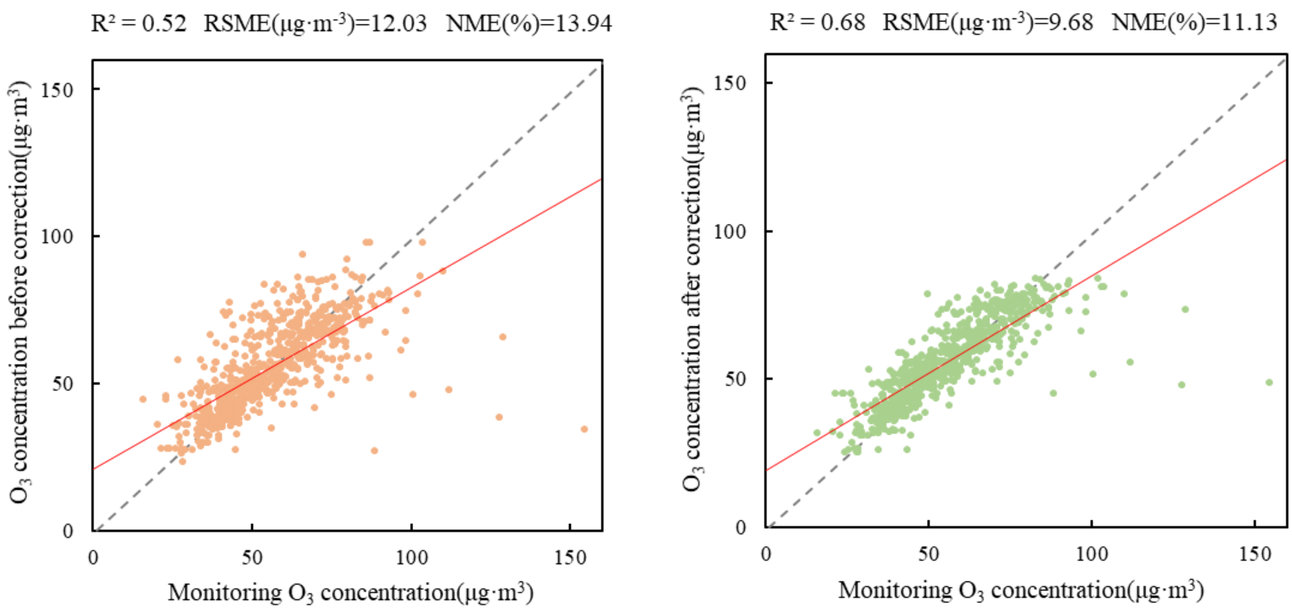

Figure A1. Correlation and statistical indexes between monthly O_3 concentration and monthly monitored O_3 concentration before and after correction.

Table A1. Meteorology, emission, and landscape pattern ecological detection results.

	WS	**SP**	**T**	**RH**	**TP**	**BC**	**CO**	**CO_2**	**NH_3**	**NO_x**
SP	N									
T	Y	Y								
RH	Y	Y	Y							
TP	Y	Y	N	Y						
BC	Y	N	Y	Y	Y					
CO	Y	N	Y	Y	Y	N				
CO_2	Y	N	Y	Y	Y	N	N			
NH_3	Y	N	Y	Y	Y	N	N	N		
NO_x	Y	N	Y	Y	Y	N	N	N	N	
OC	Y	N	Y	Y	Y	N	N	N	N	N
$PM_{2.5}$	Y	N	Y	Y	Y	N	N	N	N	N
PM_{10}	Y	N	Y	Y	Y	N	N	N	N	N
SO_2	Y	N	Y	Y	Y	N	N	N	N	N
VOC	Y	N	Y	Y	Y	N	N	N	N	N
LPI	Y	N	Y	Y	Y	N	N	N	N	N
LSI	Y	N	Y	Y	Y	N	N	N	N	N
SHAPE MN	Y	N	Y	Y	Y	N	N	N	N	N
CONTAG	Y	N	Y	Y	Y	N	N	N	N	N
SHDI	Y	N	Y	Y	Y	N	N	N	N	N
AI	Y	N	Y	Y	Y	N	N	N	N	N
	OC	**$PM_{2.5}$**	**PM_{10}**	**SO_2**	**VOC**	**LPI**	**LSI**	**SHAPE MN**	**CONTAG**	**SHDI**
$PM_{2.5}$	N									
PM_{10}	N	N								
SO_2	N	N	N							
VOC	N	N	N	N						
LPI	N	N	N	N	N					
LSI	N	N	N	N	N	N				
SHAPE MN	N	N	N	N	N	N	N			
CONTAG	N	N	N	N	N	N	N	N		
SHDI	N	N	N	N	N	N	N	N	N	
AI	N	N	N	N	N	N	N	N	N	N

Note: Y indicates that there is a significant difference in the effects of the two factors on O_3 changes, and N means no significant difference.

Table A2. The q and *p* values of factor detectors for O_3 concentration and landscape patterns at different wind speed classes (*p*-values less than 0.01 represent results significant at the 0.01 level).

	WS (1–2)		**WS (1–2)**		**WS (5–6)**		**WS (7–8)**		**WS (9–10)**	
	q	***p***	**q**	***p***	**q**	***p***	**q**	***p***	**q**	***p***
LPI	0.02	0.81	0.01	0.99	0.04	0.93	0.07	0.99	0.10	1.00
LSI	0.03	0.83	0.00	1.00	0.06	0.74	0.06	1.00	0.10	1.00
SHAPE MN	0.01	1.00	0.02	1.00	0.05	0.97	0.06	0.89	0.10	1.00
CONTAG	0.02	1.00	0.02	0.99	0.03	1.00	0.07	0.69	0.10	1.00
SHDI	0.02	0.98	0.03	0.70	0.05	1.00	0.04	0.97	0.08	1.00
AI	0.03	1.00	0.01	1.00	0.03	1.00	0.08	0.91	0.07	1.00

References

1. World Health Organization. *Air Quality Guidelines: Global Update 2005: Particulate Matter, Ozone, Nitrogen Dioxide, and Sulfur Dioxide*; World Health Organization: Geneva, Switzerland, 2006.
2. Zhao, N.; Pinault, L.; Toyib, O.; Vanos, J.; Tjepkema, M.; Cakmak, S. Long-term ozone exposure and mortality from neurological diseases in Canada. *Environ. Int.* **2021**, *157*, 106817. [CrossRef]
3. Mahmood, F.; Khokhar, M.F.; Mahmood, Z. Examining the relationship of tropospheric ozone and climate change on crop productivity using the multivariate panel data techniques. *J. Environ. Manag.* **2020**, *272*, 111024. [CrossRef]
4. Maji, K.J.; Ye, W.-F.; Arora, M.; Nagendra, S.M.S. Ozone pollution in Chinese cities: Assessment of seasonal variation, health effects and economic burden. *Environ. Pollut.* **2019**, *247*, 792–801. [CrossRef] [PubMed]

5. Ugalde-Resano, R.; Riojas-Rodríguez, H.; Texcalac-Sangrador, J.L.; Cruz, J.C.; Hurtado-Díaz, M. Short term exposure to ambient air pollutants and cardiovascular emergency department visits in Mexico city. *Environ. Res.* **2022**, *207*, 112600. [CrossRef] [PubMed]
6. Wang, Z.-b.; Li, J.-x.; Liang, L.-w. Spatio-temporal evolution of ozone pollution and its influencing factors in the Beijing-Tianjin-Hebei Urban Agglomeration. *Environ. Pollut.* **2020**, *256*, 113419. [CrossRef] [PubMed]
7. *The 2016 Report on the State of the Ecology and Environment in China*; Ministry of Ecology and Environment of People's Republic of China: Beijing, China, 2017.
8. *The 2017 Report on the State of the Ecology and Environment in China*; Ministry of Ecology and Environment of People's Republic of China: Beijing, China, 2018.
9. *The 2018 Report on the State of the Ecology and Environment in China*; Ministry of Ecology and Environment of People's Republic of China: Beijing, China, 2019.
10. *The 2019 Report on the State of the Ecology and Environment in China*; Ministry of Ecology and Environment of People's Republic of China: Beijing, China, 2020.
11. Silver, B.; Reddington, C.L.; Arnold, S.R.; Spracklen, D.V. Substantial changes in air pollution across China during 2015–2017. *Environ. Res. Lett.* **2018**, *13*, 114012. [CrossRef]
12. Liu, Y.; Wang, T. Worsening urban ozone pollution in China from 2013 to 2017–Part 2: The effects of emission changes and implications for multi-pollutant control. *Atmos. Chem. Phys.* **2020**, *20*, 6323–6337. [CrossRef]
13. Mousavinezhad, S.; Choi, Y.; Pouyaei, A.; Ghahremanloo, M.; Nelson, D.L. A comprehensive investigation of surface ozone pollution in China, 2015–2019: Separating the contributions from meteorology and precursor emissions. *Atmos. Res.* **2021**, *257*, 105599. [CrossRef]
14. Chen, Z.; Li, R.; Chen, D.; Zhuang, Y.; Gao, B.; Yang, L.; Li, M. Understanding the causal influence of major meteorological factors on ground ozone concentrations across China. *J. Clean. Prod.* **2020**, *242*, 118498. [CrossRef]
15. Han, H.; Liu, J.; Shu, L.; Wang, T.; Yuan, H. Local and synoptic meteorological influences on daily variability in summertime surface ozone in eastern China. *Atmos. Chem. Phys.* **2020**, *20*, 203–222. [CrossRef]
16. Liu, P.; Song, H.; Wang, T.; Wang, F.; Li, X.; Miao, C.; Zhao, H. Effects of meteorological conditions and anthropogenic precursors on ground-level ozone concentrations in Chinese cities. *Environ. Pollut.* **2020**, *262*, 114366. [CrossRef] [PubMed]
17. Ma, M.; Yao, G.; Guo, J.; Bai, K. Distinct spatiotemporal variation patterns of surface ozone in China due to diverse influential factors. *J. Environ. Manag.* **2021**, *288*, 112368. [CrossRef] [PubMed]
18. Tang, G.; Wang, Y.; Li, X.; Ji, D.; Hsu, S.; Gao, X. Spatial-temporal variations in surface ozone in Northern China as observed during 2009–2010 and possible implications for future air quality control strategies. *Atmos. Chem. Phys.* **2012**, *12*, 2757–2776. [CrossRef]
19. World Health Organization. *WHO Global Air Quality Guidelines: Particulate Matter ($PM_{2.5}$ and PM_{10}), Ozone, Nitrogen Dioxide, Sulfur Dioxide and Carbon Monoxide*; World Health Organization: Geneva, Switzerland, 2021.
20. Chen, Z.; Zhuang, Y.; Xie, X.; Chen, D.; Cheng, N.; Yang, L.; Li, R. Understanding long-term variations of meteorological influences on ground ozone concentrations in Beijing During 2006–2016. *Environ. Pollut.* **2019**, *245*, 29–37. [CrossRef]
21. Fu, Y.; Tai, A.P.K. Impact of climate and land cover changes on tropospheric ozone air quality and public health in East Asia between 1980 and 2010. *Atmos. Chem. Phys.* **2015**, *15*, 10093–10106. [CrossRef]
22. Lu, D.; Xu, J.; Yue, W.; Mao, W.; Yang, D.; Wang, J. Response of $PM_{2.5}$ pollution to land use in China. *J. Clean. Prod.* **2020**, *244*, 118741.
23. Tu, M.; Liu, Z.; He, C.; Fang, Z.; Lu, W. The relationships between urban landscape patterns and fine particulate pollution in China: A multiscale investigation using a geographically weighted regression model. *J. Clean. Prod.* **2019**, *237*, 117744. [CrossRef]
24. Yang, H.; Chen, W.; Liang, Z. Impact of land use on $PM_{2.5}$ pollution in a representative city of middle China. *Int. J. Environ. Res. Public Health* **2017**, *14*, 462.
25. Cheng, J.; Su, J.; Cui, T.; Li, X.; Dong, X.; Sun, F.; Yang, Y.; Tong, D.; Zheng, Y.; Li, Y. Dominant role of emission reduction in $PM_{2.5}$ air quality improvement in Beijing during 2013–2017: A model-based decomposition analysis. *Atmos. Chem. Phys.* **2019**, *19*, 6125–6146. [CrossRef]
26. Li, K.; Jacob, D.J.; Liao, H.; Zhu, J.; Shah, V.; Shen, L.; Bates, K.H.; Zhang, Q.; Zhai, S. A two-pollutant strategy for improving ozone and particulate air quality in China. *Nat. Geosci.* **2019**, *12*, 906–910. [CrossRef]
27. Liu, T.; Gong, S.; He, J.; Yu, M.; Wang, Q.; Li, H.; Liu, W.; Zhang, J.; Li, L.; Wang, X. Attributions of meteorological and emission factors to the 2015 winter severe haze pollution episodes in China's Jing-Jin-Ji area. *Atmos. Chem. Phys.* **2017**, *17*, 2971–2980. [CrossRef]
28. Zhang, W.; Wang, H.; Zhang, X.; Peng, Y.; Zhong, J.; Wang, Y.; Zhao, Y. Evaluating the contributions of changed meteorological conditions and emission to substantial reductions of $PM_{2.5}$ concentration from winter 2016 to 2017 in Central and Eastern China. *Sci. Total Environ.* **2020**, *716*, 136892. [PubMed]
29. AlOmar, M.K.; Hameed, M.M.; AlSaadi, M.A. Multi hours ahead prediction of surface ozone gas concentration: Robust artificial intelligence approach. *Atmos. Pollut. Res.* **2020**, *11*, 1572–1587. [CrossRef]
30. Su, X.; An, J.; Zhang, Y.; Zhu, P.; Zhu, B. Prediction of ozone hourly concentrations by support vector machine and kernel extreme learning machine using wavelet transformation and partial least squares methods. *Atmos. Pollut. Res.* **2020**, *11*, 51–60. [CrossRef]

31. Otero, N.; Sillmann, J.; Schnell, J.L.; Rust, H.W.; Butler, T. Synoptic and meteorological drivers of extreme ozone concentrations over Europe. *Environ. Res. Lett.* **2016**, *11*, 024005. [CrossRef]
32. Sharma, A.; Mandal, T.K.; Sharma, S.K.; Shukla, D.K.; Singh, S. Relationships of surface ozone with its precursors, particulate matter and meteorology over Delhi. *J. Atmos. Chem.* **2017**, *74*, 451–474. [CrossRef]
33. Zhao, W.; Fan, S.; Guo, H.; Gao, B.; Sun, J.; Chen, L. Assessing the impact of local meteorological variables on surface ozone in Hong Kong during 2000–2015 using quantile and multiple line regression models. *Atmos. Environ.* **2016**, *144*, 182–193. [CrossRef]
34. Cheng, N.; Li, R.; Xu, C.; Chen, Z.; Chen, D.; Meng, F.; Cheng, B.; Ma, Z.; Zhuang, Y.; He, B. Ground ozone variations at an urban and a rural station in Beijing from 2006 to 2017: Trend, meteorological influences and formation regimes. *J. Clean. Prod.* **2019**, *235*, 11–20. [CrossRef]
35. Chen, Y.; Yan, H.; Yao, Y.; Zeng, C.; Gao, P.; Zhuang, L.; Fan, L.; Ye, D. Relationships of ozone formation sensitivity with precursors emissions, meteorology and land use types, in Guangdong-Hong Kong-Macao Greater Bay Area, China. *J. Environ. Sci.* **2020**, *94*, 1–13. [CrossRef]
36. Camalier, L.; Cox, W.; Dolwick, P. The effects of meteorology on ozone in urban areas and their use in assessing ozone trends. *Atmos. Environ.* **2007**, *41*, 7127–7137. [CrossRef]
37. Taylan, O. Modelling and analysis of ozone concentration by artificial intelligent techniques for estimating air quality. *Atmos. Environ.* **2017**, *150*, 356–365. [CrossRef]
38. Zhang, Y.H.; Su, H.; Zhong, L.J.; Cheng, Y.F.; Zeng, L.M.; Wang, X.S.; Xiang, Y.R.; Wang, J.L.; Gao, D.F.; Shao, M. Regional ozone pollution and observation-based approach for analyzing ozone–precursor relationship during the PRIDE-PRD2004 campaign. *Atmos. Environ.* **2008**, *42*, 6203–6218. [CrossRef]
39. Reddy, B.S.K.; Kumar, K.R.; Balakrishnaiah, G.; Gopal, K.R.; Reddy, R.R.; Ahammed, Y.N.; Narasimhulu, K.; Reddy, L.S.S.; Lal, S. Observational studies on the variations in surface ozone concentration at Anantapur in southern India. *Atmos. Res.* **2010**, *98*, 125–139. [CrossRef]
40. He, B.-J.; Wang, J.; Zhu, J.; Qi, J. Beating the urban heat: Situation, background, impacts and the way forward in China. *Renew. Sustain. Energy Rev.* **2022**, *161*, 112350. [CrossRef]
41. Guo, H.; Ling, Z.; Cheng, H.; Simpson, I.; Lyu, X.; Wang, X.; Shao, M.; Lu, H.; Ayoko, G.; Zhang, Y. Tropospheric volatile organic compounds in China. *Sci. Total Environ.* **2017**, *574*, 1021–1043. [CrossRef]
42. Tang, X.; Kong, L.; Zhu, J.; Wang, Z.; Li, J.; Wu, H.; Wu, Q.; Chen, H.; Zhu, L.; Wang, W. *A High-Resolution Air Quality Reanalysis Dataset over China (CAQRA)*; Science Data Bank: Beijing, China, 2021.
43. Kong, L.; Tang, X.; Zhu, J.; Wang, Z.; Li, J.; Wu, H.; Wu, Q.; Chen, H.; Zhu, L.; Wang, W. A 6-year-long (2013–2018) high-resolution air quality reanalysis dataset in China based on the assimilation of surface observations from CNEMC. *Earth Syst. Sci. Data* **2021**, *13*, 529–570. [CrossRef]
44. McNoldy, B. Temperature, Dewpoint, and Relative Humidity Calculator. Available online: http://bmcnoldy.rsmas.miami.edu/Humidity.html (accessed on 12 November 2021).
45. Guo, Z.; Wang, C.; Liu, X.; Pang, G.; Zhu, M.; Yang, L. Accuracy assessment of the from-Glc30 land cover dataset based on watershed sampling units: A continental-scale study. *Sustainability* **2020**, *12*, 8435. [CrossRef]
46. Liang, S.; Li, X.; Teng, Y.; Fu, H.; Chen, L.; Mao, J.; Zhang, H.; Gao, S.; Sun, Y.; Ma, Z. Estimation of health and economic benefits based on ozone exposure level with high spatial-temporal resolution by fusing satellite and station observations. *Environ. Pollut.* **2019**, *255*, 113267. [CrossRef]
47. Wang, J.F.; Xu, C.D. Geodetector: Principle and prospective. *Acta Geogr. Sin.* **2017**, *72*, 116–134.
48. Yin, C.; Deng, X.; Zou, Y.; Solmon, F.; Li, F.; Deng, T. Trend analysis of surface ozone at suburban Guangzhou, China. *Sci. Total Environ.* **2019**, *695*, 133880. [CrossRef]
49. Yang, L.; Luo, H.; Yuan, Z.; Zheng, J.; Huang, Z.; Li, C.; Lin, X.; Louie, P.K.K.; Chen, D.; Bian, Y. Quantitative impacts of meteorology and precursor emission changes on the long-term trend of ambient ozone over the Pearl River Delta, China, and implications for ozone control strategy. *Atmos. Chem. Phys.* **2019**, *19*, 12901–12916. [CrossRef]
50. Lee, Y.C.; Chan, K.L.; Wenig, M.O. Springtime warming and biomass burning causing ozone episodes in South and Southwest China. *Air Qual. Atmos. Health* **2019**, *12*, 919–931. [CrossRef]
51. Chan, C.; Chan, L.; Chang, W.; Zheng, Y.; Cui, H.; Zheng, X.; Qin, Y.; Li, Y.S. Characteristics of a tropospheric ozone profile and implications for the origin of ozone over subtropical China in the spring of 2001. *J. Geophys. Res. Atmos.* **2003**, *108*, 8800. [CrossRef]
52. Chan, C.Y.; Chan, L.Y.; Harris, J.M.; Oltmans, S.J.; Blake, D.R.; Qin, Y.; Zheng, Y.G.; Zheng, X.D. Characteristics of biomass burning emission sources, transport, and chemical speciation in enhanced springtime tropospheric ozone profile over Hong Kong. *J. Geophys. Res. Atmos.* **2003**, *108*, ACH3-1–ACH3-13. [CrossRef]
53. Ge, C.; Liu, J.; Cheng, X.; Fang, K.; Chen, Z.; Chen, Z.; Hu, J.; Jiang, D.; Shen, L.; Yang, M. Impact of regional transport on high ozone episodes in southeast coastal regions of China. *Atmos. Pollut. Res.* **2022**, *13*, 101497. [CrossRef]
54. Wang, Y.; Du, H.; Xu, Y.; Lu, D.; Wang, X.; Guo, Z. Temporal and spatial variation relationship and influence factors on surface urban heat island and ozone pollution in the Yangtze River Delta, China. *Sci. Total Environ.* **2018**, *631*, 921–933. [CrossRef]
55. Ouyang, S.; Deng, T.; Liu, R.; Chen, J.; He, G.; Leung, J.C.-H.; Wang, N.; Liu, S.C. Impact of a subtropical high and a typhoon on a severe ozone pollution episode in the Pearl River Delta, China. *Atmos. Chem. Phys. Discuss.* **2022**, *22*, 10751–10767. [CrossRef]

56. Deng, T.; Wang, T.; Wang, S.; Zou, Y.; Yin, C.; Li, F.; Liu, L.; Wang, N.; Song, L.; Wu, C. Impact of typhoon periphery on high ozone and high aerosol pollution in the Pearl River Delta region. *Sci. Total Environ.* **2019**, *668*, 617–630. [CrossRef]
57. Gong, S.; Liu, Y.; He, J.; Zhang, L.; Lu, S.; Zhang, X. Multi-scale analysis of the impacts of meteorology and emissions on $PM_{2.5}$ and O_3 trends at various regions in China from 2013 to 2020 1: Synoptic circulation patterns and pollution. *Sci. Total Environ.* **2022**, *815*, 152770. [CrossRef]
58. Zhang, X.; Xiao, X.; Wang, F.; Brasseur, G.; Chen, S.; Wang, J.; Gao, M. Observed sensitivities of $PM_{2.5}$ and O_3 extremes to meteorological conditions in China and implications for the future. *Environ. Int.* **2022**, *168*, 107428.
59. Dadashpoor, H.; Azizi, P.; Moghadasi, M. Land use change, urbanization, and change in landscape pattern in a metropolitan area. *Sci. Total Environ.* **2019**, *655*, 707–719. [CrossRef]
60. Cardelino, C.; Chameides, W. Natural hydrocarbons, urbanization, and urban ozone. *J. Geophys. Res. Atmos.* **1990**, *95*, 13971–13979. [CrossRef]
61. Khiem, M.; Ooka, R.; Huang, H.; Hayami, H.; Yoshikado, H.; Kawamoto, Y. Analysis of the relationship between changes in meteorological conditions and the variation in summer ozone levels over the Central Kanto area. *Adv. Meteorol.* **2010**, *2010*, 349248. [CrossRef]
62. Li, M.; Song, Y.; Mao, Z.; Liu, M.; Huang, X. Impacts of thermal circulations induced by urbanization on ozone formation in the Pearl River Delta region, China. *Atmos. Environ.* **2016**, *127*, 382–392. [CrossRef]
63. Tong, N.Y.O.; Leung, D.Y.C.; Liu, C.-H. A review on ozone evolution and its relationship with boundary layer characteristics in urban environments. *Water Air Soil Pollut.* **2011**, *214*, 13–36. [CrossRef]
64. Chen, Z.; Cai, J.; Gao, B.; Xu, B.; Dai, S.; He, B.; Xie, X. Detecting the causality influence of individual meteorological factors on local $PM_{2.5}$ concentration in the Jing-Jin-Ji region. *Sci. Rep.* **2017**, *7*, 40735. [CrossRef]
65. Wang, T.; Xue, L.; Brimblecombe, P.; Lam, Y.F.; Li, L.; Zhang, L. Ozone pollution in China: A review of concentrations, meteorological influences, chemical precursors, and effects. *Sci. Total Environ.* **2017**, *575*, 1582–1596. [CrossRef]
66. Shi, B.; Yuan, X.; Zheng, C.; Yu, Y.; Huang, Z.; Zheng, J. VOC emission caps constrained by air quality targets based on response surface model: A case study in the Pearl River Delta Region, China. *J. Environ. Sci.* 2022; *in press*.
67. Latha, K.M.; Badarinath, K.V.S. Correlation between black carbon aerosols, carbon monoxide and tropospheric ozone over a tropical urban site. *Atmos. Res.* **2004**, *71*, 265–274. [CrossRef]
68. Gao, J.; Zhu, B.; Xiao, H.; Kang, H.; Pan, C.; Wang, D.; Wang, H. Effects of black carbon and boundary layer interaction on surface ozone in Nanjing, China. *Atmos. Chem. Phys.* **2018**, *18*, 7081–7094. [CrossRef]
69. Lim, H.-J.; Turpin, B.J. Origins of primary and secondary organic aerosol in Atlanta: Results of time-resolved measurements during the Atlanta supersite experiment. *Environ. Sci. Technol.* **2002**, *36*, 4489–4496. [CrossRef]
70. Deng, X.; Tie, X.; Zhou, X.; Wu, D.; Zhong, L.; Tan, H.; Li, F.; Huang, X.; Bi, X.; Deng, T. Effects of Southeast Asia biomass burning on aerosols and ozone concentrations over the Pearl River Delta (PRD) region. *Atmos. Environ.* **2008**, *42*, 8493–8501. [CrossRef]
71. Cheng, H.; Guo, H.; Saunders, S.; Lam, S.; Jiang, F.; Wang, X.; Simpson, I.; Blake, D.; Louie, P.; Wang, T. Assessing photochemical ozone formation in the Pearl River Delta with a photochemical trajectory model. *Atmos. Environ.* **2010**, *44*, 4199–4208. [CrossRef]
72. Guo, H.; Cheng, H.; Ling, Z.; Louie, P.; Ayoko, G. Which emission sources are responsible for the volatile organic compounds in the atmosphere of Pearl River Delta? *J. Hazard. Mater.* **2011**, *188*, 116–124. [CrossRef] [PubMed]
73. Jin, X.; Holloway, T. Spatial and temporal variability of ozone sensitivity over China observed from the Ozone Monitoring Instrument. *J. Geophys. Res. Atmos.* **2015**, *120*, 7229–7246. [CrossRef]